Applied Catalysis A, General 571 (2019) 82–88

Contents lists available at ScienceDirect

Applied Catalysis A, General

journal homepage: www.elsevier.com/locate/apcata

# Nanodiamond@carbon nitride hybrid with loose porous carbon nitride layers as an efficient metal-free catalyst for direct dehydrogenation of ethylbenzene

Guifang Ge, Zhongkui Zhao*

*State Key Laboratory of Fine Chemicals, Department of Catalysis Chemistry and Engineering, School of Chemical Engineering, Dalian University of Technology, 2 Linggong Road, Dalian, 116024, China*

ARTICLE INFO

*Keywords:*
Hybrid
Nanodiamond
Dispersant and precursor
Direct dehydrogenation
Defects and ketonic carbonyl groups

ABSTRACT

This work presents a facile and low-cost approach to prepare nanodiamond@carbon nitride hybrid with loose porous carbon nitride layers close wrapped on well dispersed NDs (ND-CN) through the thermal polymerization of the mixture composed of hexamethylenetetramine (HTM) and ammonium chloride adsorbed on dispersed nanodiamonds (ND), in which hexamethylenetetramine serves as both carbon nitride precursor and dispersing agent and the ammonium chloride acts as gas template. ND-CN shows 1.9 and 1.2 times much higher styrene rate for oxygen and steam-free direct dehydrogenation of ethylbenzene than the pristine ND and the previously reported carbon nitride layers encapsulated ND (H-ND) formed by the thermal polymerization of mixture composed of HTM and ND, respectively, ascribed the more exposed active sites containing structural defects and ketonic carbonyl groups and the not weakened synergistic effect of carbon nitride with ND that originating from the enlarging surface area and pore volume owing to the characteristic concerning loose porous structure of carbon nitride layers.

## 1. Introduction

Nanocarbon materials have attracted continuous interest in many fields including batteries, electrochemical energy storage and catalysis [1–3], due to their good corrosion resistance, stable structure and excellent surface chemistry [4,5]. Among which, nanodiamond (ND) is a distinctive material for its unique $sp^2$-$sp^3$ hybridized structure, extreme hardness and chemical stability [6], which bring up its wide application in drug delivery, electrocatalyst and metal-free catalysis [7–9]. And it was demonstrated that ND can be employed for oxygen and steam-free direct dehydrogenation (DDH) of ethylbenzene to styrene, Su and co-workers have revealed the much superior catalytic activity and great potential of ND regarding of direct dehydrogenation of ethylbenzene than that of the commercial potassium-iron catalyst for industrial application [10]. A number of nanostructured carbon materials such as nanodiamond/CNT-SiC [11], nanodiamond/nitrogen-doped mesoporous carbon [12], nitride-doped carbon nanotube [13], and nanodiamond/grapheme [14,15] have previously been shown to be effective in enhancing the DDH of ethylbenzene in recent years. Our group (Advanced Catalytic Material Research Group), DUT, have developed a two-step method to synthesize a ND closely wrapped with carbon nitride layer (H-ND) [16]. ND powder and hexamethylenetetramine were milled to be well mixed, and then to be pyrolyzed. The H-ND displayed a higher and more stable activity than M-ND manufactured from ND with melamine [17] for steam-free DDH of ethylbenzene to styrene. The existence of synergistic effect between ND and carbon nitride accounted for the good DDH performance. However, a large amount of active sites of ND was also closely-wrapped and covered by carbon nitride layer and that depressed catalytic performance. Therefore, we envision that the ND-CN hybrid with loose and porous carbon nitride layers closely encapsulating on ND surface may exhibit outstanding catalytic performance in DDH of ethylbenzene owing to the maintained strong synergistic effect of ND can carbon nitrides but not decreasing the accessibility of active sites.

Recent studies have demonstrated that the surface structural defects and ketonic carbonyl groups are active sites for C—H activation [18,19]. Surface defects not only endow the materials with more exposed active edges but also provide a large number of boundaries thus reduce aggregation. On the other hand, it is necessary to generate more defects for the sake of higher catalytic performance. A variety of tactics including alkali-assisted route [20,21], thermal polymerization with precursors [22] and gas etching [23] were utilized to yield defects.

* Corresponding author.
*E-mail address:* zkzhao@dlut.edu.cn (Z. Zhao).

https://doi.org/10.1016/j.apcata.2018.12.016
Received 7 September 2018; Received in revised form 13 December 2018; Accepted 14 December 2018
Available online 14 December 2018
0926-860X/ 

Ammonium chloride has also been employed to introducing defects [24]. $NH_3$ and HCl pyrolyzed from ammonium chloride act as soft template to produce porous structure and surface defects from $NH_3$ solely [25].

Herein, we introduce ammonium chloride to produce ND@carbon nitride with loose porous carbon nitride structure to release more active sites that belong to ND, but not weaken the synergistic effect between the ND and the encapsulated carbon nitrides on ND. Compared with the approaches previously reported [16], besides the strong synergistic effect of ND and carbon nitride layers owing to the carbon nitride layers close wrapped on ND led by the unique molecular structure of HTM, in the developed wet-mixing of ND with HTM, and HTM can also act as dispersing agent to allow the ND well being dispersed. Moreover, the introduced ammonium chloride serves as gas template to produce pores and defect. As a consequence, nanodiamond@carbon nitride hybrid with loose porous carbon nitride layers close wrapped on well dispersed NDs (ND-CN) was successfully prepared. ND-CN shows 1.9 and 1.2 times much higher styrene rate for oxygen and steam-free direct dehydrogenation of ethylbenzene than the pristine ND and the previously reported carbon nitride encapsulated ND (H-ND) formed by the thermal polymerization of mixture composed of HTM and ND, respectively, ascribed the increased active sites containing defects and ketonic carbonyl groups and the not weakened synergistic effect of carbon nitride with ND that originating from the enlarging surface area and pore volume owing to the characteristic concerning loose porous structure of carbon nitride layers.

## 2. Experimental

### 2.1. Catalysts preparation

Commercially available nanodiamond from Beijing Grish Hitech Co. (China) were treated in acid solution, and then obtained oxidized nanodiamond (O-ND). ND-CN was synthesized as follows: 0.25 g HTM and $NH_4Cl$ were dissolved in 20 ml deionized $H_2O$. Next, O-ND was added into the mixture, and then treated by further ultrasonication. The water was removed under the reduced pressure, subsequently placed in a quartz tube filled with flowing $N_2$ at 750 °C. The preparation method of Carbon nitride (CN) is same as above, but no ND is introduced. H-ND was obtained by a method described in a previous report [16].

### 2.2. Catalysts characterization

X-ray diffraction (XRD) profiles were collected from 10 to 80° at a step width of 0.02° using Rigaku Automatic X-ray Diffractometer (D/Max 2400) equipped with a CuKa source (λ = 1.5406 Å). Field emission scanning electron microscope (FESEM) experiments were performed on JEOL JSM-5600LV SEM/EDX instrument. Transmission electron microscopy (TEM) images were obtained by using Tecnai F30 HRTEM instrument (FEI Corp.) at an acceleration voltage of 300 kV. The XPS spectra were carried out on an ESCALAB 250 XPS system with a monochromatized Al Ka X-ray source (15 kV, 150 W, 500 μm, pass energy = 50 eV). The Raman spectra were measured using a laser with an excitation wavelength of 532 nm at room temperature on a Thermo Scientific DXR Raman microscope. Nitrogen adsorption and desorption isotherms were determined on a Micromeritics apparatus of model ASAP-2050 system at −196 °C. The specific surface areas were calculated by the BET method and the pore size distributions were calculated from adsorption branch of the isotherm by BJH model. Note: the catalysts after 20 h reaction were characterized because we compared the steady state catalytic performance (steady state styrene rate and selectivity) of catalysts after the 20 h of time of stream.

### 2.3. Catalytic performance measurement

The oxidant- and steam-free direct dehydrogenation of ethylbenzene was performed over the developed catalyst and the experimental details are as follows: the reaction was performed at 550 °C for 20 h in a stainless steel, fixed bed flow reactor (6 mm O.D.). 25 mg catalyst was loaded at the centre of the reactor with two quartz wool plugs at its two sides. The system was heated to 600 °C and kept for 30 min in Ar for pretreating catalyst. After the system was cooled down to 550 °C and kept for 10 min, the feed containing 2.8% ethylbenzene with 10 ml $min^{-1}$ of gas hourly space velocity (GHSV) and Ar as balance was then fed into the reactor from a saturator kept at 40 °C. The effluent from the reactor was condensed in two traps containing certain amount of ethanol connected in a series. The condensed material was cooled externally in an ice water bath. Quantitative analysis of the collected reaction products (ethylbenzene, styrene, toluene, and benzene) was performed on a FULI 9790 II GC equipped with HP-5 column, 30 m × 0.32 mm × 0.25 μm, and FID detector. The resulting carbon balance was above 100 ± 4% in all reactions. The selectivity of styrene is employed as the evaluation standard for the catalytic performance of the fabricated catalysts. The styrene rate is calculated as the formed styrene molar amount per g catalyst per hour, and the selectivity of styrene is denoted as the percentage of the desired styrene to the total products including the desired styrene and the by-products that containing benzene and toluene. The variation of conversion and selectivity with contact time was measured by changing the GHSV from 6 to 14 ml $min^{-1}$ with a step of 2 ml $min^{-1}$. The contact time is denoted as the volume of catalyst being divided by $GHSV_{EB}$, in which the GHSV multiplies ethylbenzene content to obtain $GHSV_{EB}$.

## 3. Results and discussion

### 3.1. Morphology and structure feature of samples

Fig. 1 presents the preparation process of the ND-CN hybrid featuring the NDs dispersed in loose porous carbon nitride structure. Firstly, the commercial ND was well dispersed by ultrasonic in solution of ammonium chloride and hexamethylenetetramine, then the followed thermal polymerization of hexamethylenetetramine in the presence of ammonium chloride. The morphology of the ND (a), H-ND (c) and ND-CN (d) was investigated by transmission electron microscopy (TEM)

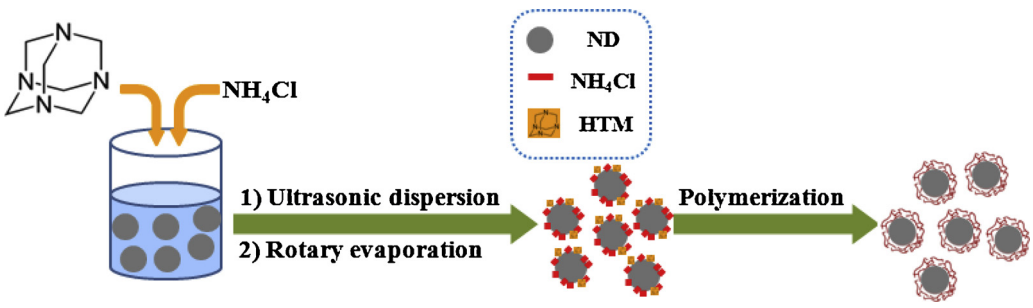


**Fig. 1.** Proposed process for the preparation of ND-CN material.

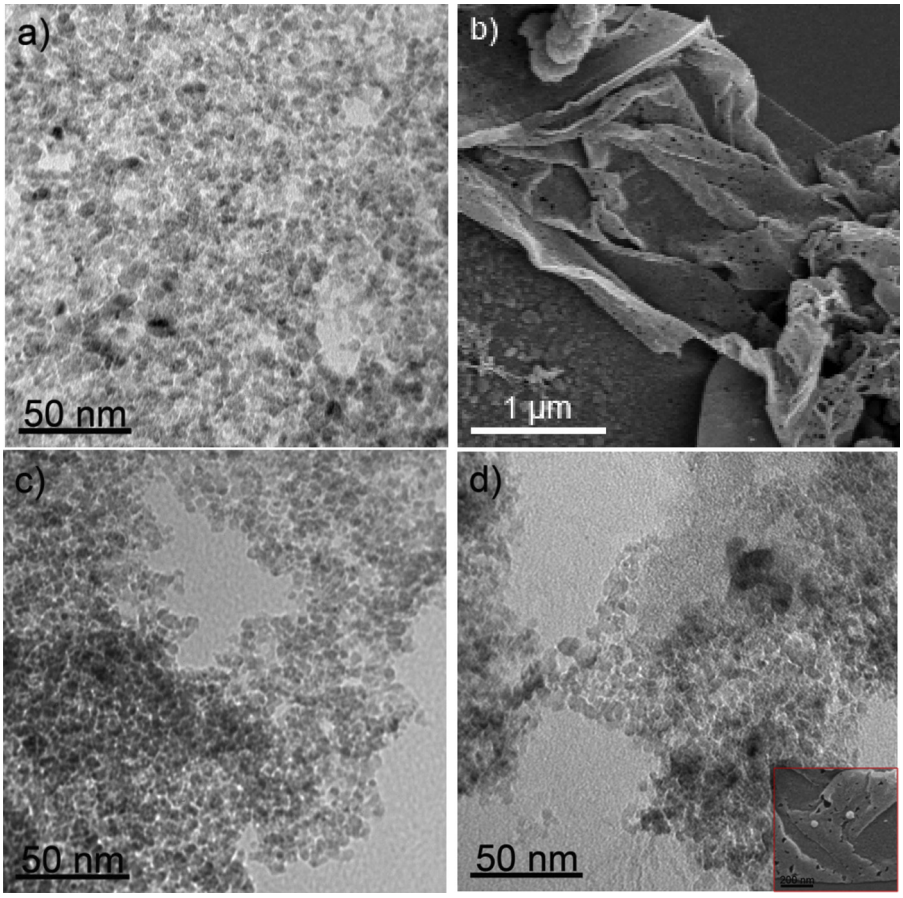


**Fig. 2.** (a) TEM images of ND. (b) FE-SEM image of CN. (c,d) TEM images of H-ND (c) and ND-CN (d). Inset in Fig. 2d: FE-SEM image of ND-CN.

and the CN (b) by field-emission scanning electron microscopy (FESEM). As shown in Fig. 2, the pristine ND is composed of particles less than 10 nm that aggregate together. Carbon nitride obtained from hexamethylenetetramine and ammonium chloride features plat piece morphology with fluffy structure, while ND is flat on carbon nitride piece to form ND-CN. Compared with the pristine ND, the ND aggregation is in a looser status in H-ND and ND-CN. From the previous report [16], the H-ND features unconsolidated carbon-nitride layer close-wrapped nanodiamond hybrid (Fig. 2c). Compared to H-ND, the as-synthesized DN-CN hybrid exhibits looser carbon nitride layers coated on nanodiamond (Fig. 2d and the inset in Fig. 2d), ascribed to the bubbling $NH_3$ and HCl gas pyrolyzed from ammonium chloride. As is presented in our previous report [16], different from the melamine, the condensation of hexamethylenetetramine takes place through the C—N splitting. The formed units can be linked with $CH_2$, and therefore the flexible carbon nitride structure can be formed, which is different from the rigid structure from melamine. The flexible carbon nitride units can be further polymerized to form the CNx layers, and therefore the CNx-layer-wrapped ND nanohybrid can be formed, which can be identified by FESEM, HRTEM, BET, XRD, and Raman analyses.

All four samples exhibit a diffraction peak at about 25.3° (Fig. 3), corresponding to the typical graphite (002) of hexagonal carbon material. The widened (002) peak indicates their amorphous and disordered stacking structure of interlayer, thus demonstrating that the CN is composed of nitrogen containing loose carbon nitride layers [16]. ND, H-ND and ND-CN have three diffraction peaks located at 43.8°, 75.5° and 91° belong to (111), (022) and (113) planes of ND respectively [17]. Compared with the pristine ND and H-ND, the further weakened and widened diffraction peaks of developed ND-CN hybrid sample demonstrate promoted ND dispersity by the introduction of CN from hexamethylenetetramine and ammonium chloride and

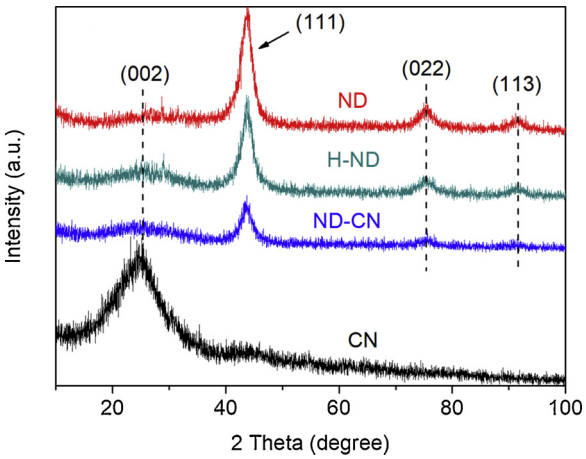


**Fig. 3.** XRD patterns of ND, H-ND, ND-CN and CN.

deaggregating effect of gas collision pyrolyzed from ammonium chloride.

In order to study the subtle structural variation of the samples, Raman spectra were performed (Fig. 4). It is well known that D band (A1g mode, disordered graphitic layer and structural defects) is centered at 1310 $cm^{-1}$, and G band (E2g mode, symmetry-allowed graphite) located at 1591 $cm^{-1}$ [26], So there is exposed graphene in all four samples. In comparison with ND, a shift of D band and of G band can be observed in H-ND, indicating the strong interaction between CN and ND, or the appearance of closely wrapped ND by carbon nitride layer, which means poor efficiency of surface carbonyl on ND [15,16]. On the contrary, no visible shift on ND-CN indicates fully exposure of

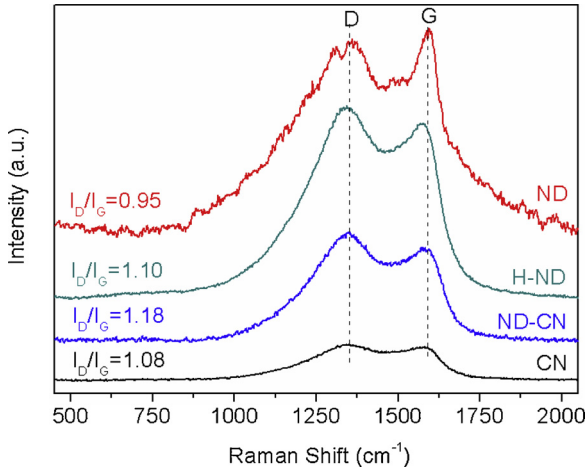


**Fig. 4.** Raman spectra of ND, H-ND, ND-CN and CN.

surface carbonyl, meanwhile fluffy carbon nitride prepared from ammonium chloride and hexamethylenetetramine can efficiently separate the aggregated ND. $I_D/I_G$ (intensity ratio of D band to G band) on ND, CN, ND-CN and H-ND was collected. due to the bubbling of $NH_3$ and HCl gases generated from ammonium chloride, the $I_D/I_G$ for ND-CN (1.1780) is remarkably higher than three other samples (0.9462 for ND, 1.0767 for CN, and 1.1004 for H-ND) and this suggests more defects and edge plane exposure in ND-CN [27], originating from the role of ammonium chloride regarding of gas template. However, the $I_D/I_G$ of CN is lower than ND-CN, although it has the highest ammonium chloride content, ascribed to the intensified gas template effect of ammonium chloride by the supporting effect of the existing MD in the mixture during pyrolysis. This is also the reason for the formation of loose carbon nitride layers in the ND-CN hybrid. Corresponded to the TEM and XRD data, Raman spectra further confirm positive actor of $NH_4Cl$ in producing carbon nitride with more defects and edge plane exposure. That is to say, the much different carbon nitride layers on ND-CN owing to the presence of ammonium chloride leads to more defects on NC-CN in comparison with H-ND and ND.

BET experiment was performed to further explore the specific surface area and pore size of ND, CN, H-ND and ND-CN (Fig. 5). The $N_2$ adsorption/desorption isotherms for all catalysts exhibit a typical IV curve, implying the presence of mesopores in all four samples. Due to the separation effect of CN (pyrolyzed from hexamethylenetetramine alone), slight improvement in surface area occurred (230.0 $m^2 g^{-1}$ for ND, 269.0 $m^2 g^{-1}$ for H-ND, Table 1). However, the surface area of ND-CN is 343.2 $m^2 g^{-1}$, since only little amount of CN (prepared from

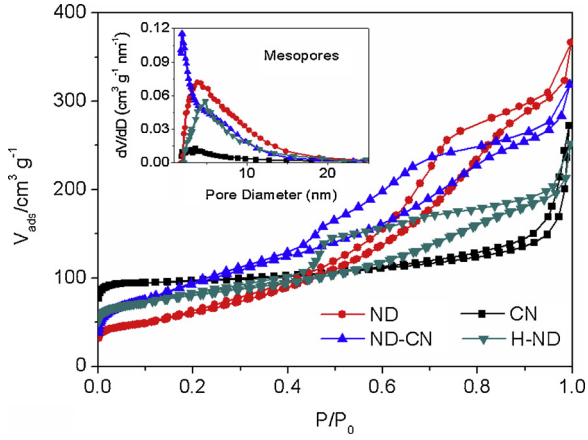


**Fig. 5.** Nitrogen adsorption-desorption isotherms. Inset: BJH mesopore size distribution of ND, CN, ND-CN and H-ND.

**Table 1**
Textural properties of the catalysts.

| Samples | $S_{BET}$[a] ($m^2 g^{-1}$) | $V_{total}$[b] ($cm^3 g^{-1}$) | $V_{micro}$[b] ($cm^3 g^{-1}$) | APS[c] (nm) |
|---|---|---|---|---|
| ND | 230.0 | 0.68 | 0.08 | 9.86 |
| CN | 306.2 | 0.42 | 0.15 | 5.50 |
| ND-CN | 343.2 | 0.49 | 0.12 | 5.75 |
| H-ND | 269.0 | 0.39 | 0.11 | 5.80 |

[a] The total surface area ($S_{total}$) was obtained from multipoint Brunauer–Emmett–Teller (BET) plots and V–t plots, respectively.
[b] The total pore volume ($V_{total}$) was determined at P/P0 = 0.99, and the micropore volume ($V_{micro}$) was calculated from the H-K plot.
[c] Average pore size (APS).

ammonium chloride and hexamethylenetetramine, surface of which is 306.2 $m^2 g^{-1}$) was introduced into the system, the enlargement of surface area may not only come from dispersion effect of CN, but also from deaggregation of the aggregated ND by the collision of formed gases from ammonium chloride. On the other hand, the gases introduced by ammonium chloride blew hexamethylenetetramine derived polymers into many large bubbles and obtain crinkly carbon nitride, and, surface defect from gas corrosion promoted ND dispersion [28]. Compared with ND-CN, the widen pore size distribution and large pore size for ND and H-ND are contributed from accumulation pores among the aggregated NDs, so although the pore volumes of ND-CN decrease from 0.68 to 0.49 $cm^3 g^{-1}$, ND is in a decentralized state in ND-CN sample. Meanwhile, a shift to smaller pore size can be observed for ND-CN's in comparison with that of ND, the smaller pores could be attributed to gases etch of ND and CN, which issues in increasing porosity and promoting dispersity. Moreover, the unique textural properties of CN-CN also imply the loose porous carbon nitride layers on ND.

XPS was employed to analyze the loading content and surface state of the four catalysts after reaction [3,29]. All four samples show dominant C peaks (284.6 eV), N peaks (400 eV) and O peaks (533 eV). The concentrations of C, N, and O are calculated and listed in Table 2. The developed ND-CN catalyst shows much different characteristic in XPS peak from the previously reported H-ND. The N/C ratios of ND, CN, ND-CN and H-ND are 0.013, 0.075, 0.027 and 0.073. The synergistic effect between the ketonic carbonyl groups on the ND and the nitrogen species comes from the electron transfer from N to C═O. The introduced electron-rich N atom can increase the nucleophilicity of C = O C═O active sites, which subsequently improve the catalytic activity of active sites for C—H activation [13–18]. The small amount of N in the commercially available ND comes from the preparation process of detonation method. The increased N content of ND-CN compared to the pristine ND would facilitate the direct dehydrogenation of ethylbenzene to styrene. The common issue is that CN has the largest N content among the samples. Interestingly, ND-CN hybrid has a lower N content than the previously reported H-ND, ascribed to the gas template role of the added ammonium chloride in the pyrolysis process. Moreover, In the C 1 s spectrum (Fig. 6b), the high resolution C 1 s spectrum can be resolved into five peaks, C═C (284.6 eV) corresponding to the graphitic structure, C—N (285.2 eV) attributed from defects on the carbon, C—C/C—O (286 eV), C═O/C = N (N-$sp^2$ C) (287 eV) and carboxyl O═ C—O (288.6 eV) [16,30]. For the CN material, the peak of C═O/C═N

**Table 2**
XPS analysis of the samples.

| Samples | N (%) | N-1 (%) | N-2 (%) | N-3 (%) | N-4 (%) | O (%) | C = O (%) | O = C-O (%) | C-O (%) |
|---|---|---|---|---|---|---|---|---|---|
| ND | 1.2 | – | 71.7 | | 28.3 | 6.9 | 63.6 | 35.0 | 1.4 |
| CN | 6.4 | 32.6 | 23.7 | 34.9 | 8.8 | 7.9 | 29.6 | 57.7 | 12.7 |
| ND-CN | 2.4 | 35.8 | 36.6 | 8.8 | 18.8 | 7.1 | 68.4 | 24.0 | 7.6 |
| H-ND | 6.3 | 53.6 | 25.0 | 11.6 | 9.8 | 7.5 | 45.6 | 31.3 | 23.1 |

N-1 (pyridinic N), N-2 (pyrrolic N), N-3 (graphitic N) and N-4 (oxidized N).

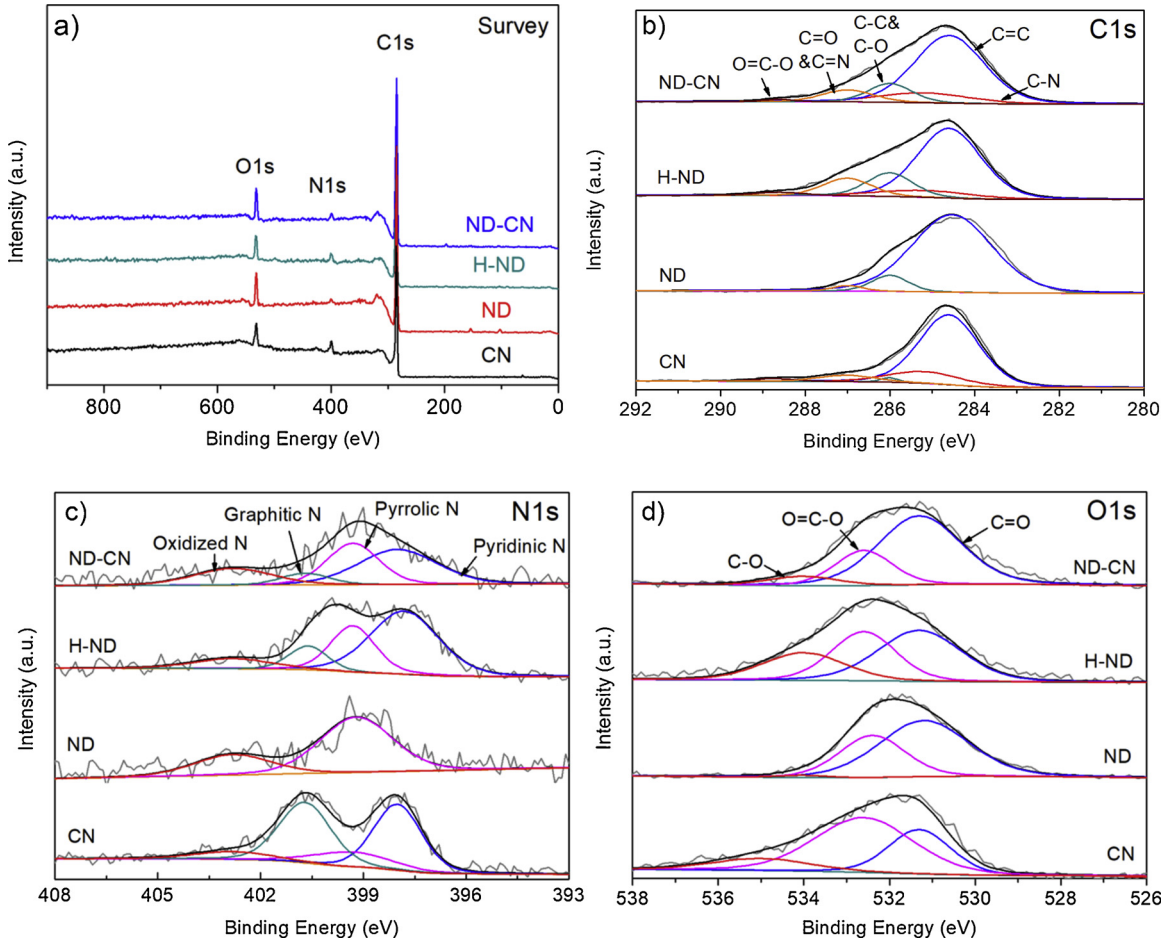


**Fig. 6.** XPS spectra of the as-prepared catalysts. (a) Survey spectra, (b) C 1 s peak, (c) N 1 s peak, and (d) O 1 s peak.

(287 eV) is weaker than that of the others, ascribed to the less C═O confirmed by the following O 1 s spectra (Fig. 6d). Compared with ND and H-ND, the C═O/C = N peak of ND-CN shows higher intensity and the C−N peaks shows smaller intensity which could be directly linked with the introduced by the surface defect transformation in the composite. From Fig. 6c, the N 1 s spectra of the catalysts can be fitted into four peaks at 398.0, 399.5, 400.8 and 402.8 eV, respectively, corresponding to the pyridinic N (C−N═C in six-atom rings at the edge of grapheme), pyrrolic N (N in the heterocyclic ring of the pentad that is attached to the phenolic or carbonyl group on the adjacent carbon atom of the ring), graphitic N ($sp^2$-hybridized N bonded to three C atoms in grapheme layer's central or valley position), and oxidized N respectively [31,32]. There are only two peaks observed at 398.0 eV (pyridinic N) and 403 eV (oxidized N) for ND, due to the absent of carbon nitride in ND. As summarized in Table 2, the pyridinic N of ND-CN is calculated to be 35.8 at% after deconvolution (Table 2), which is lower than that of H-ND (53.6 at%) and CN (32.6 at%), but the content of pyrrolic N on ND-CN is higher than H-ND. These results indicate the surface of ND-CN exit more defects under the double blast attack of hexamethylenetetramine and ammonium chloride. As to the chemical bond types of oxygen, the detailed information were obtained in Fig. 6d, the deconvoluted peaks located at 530.8, 532.5 and 533.8 eV in the O 1 s spectra are attributed to ketonic carbonyl group (C═O), O═C−O (oxygen atom in ester, anhydrides and carboxylic acid) and C−O in phenol/ether, respectively [33,34]. Total surface oxygen contents are 6.9at%, 7.9 at%, 7.1 at% and 7.5 at% for ND, CN, ND-CN and H-ND, respectively. The higher O content on the developed ND-CN than ND may be resulted from either the surface carbon nitride layers or the increased exposure of O on the ND surface. The presence of O species of CN may from oxidation of surface defects and edges by air [35,36]. Furthermore, the surface carbonyl group is the active species for direct dehydrogenation reaction [19], and the percentage contents of O concerning C═O group in the surface O are 63.6 at%, 29.6 at%, 68.4 at% and 45.6 at% for ND, CN, ND-CN and H-ND. The higher carbonyl group content of ND-CN can be observed in comparison with H-ND, which might attribute from the increased accessibility of surface O on ND owing to the more loose and porous carbon nitride layers and/or increased surface defect of ND-CN nanohybrid to form C═O led by the gas template role of ammonium chloride. The gas release from ammonium chloride destroys the integrity of the graphene basal plane and creates more edges [37].

The aforementioned results and analysis demonstrate the formation of nanodiamond@carbon nitride hybrid with loose porous carbon nitride layers close wrapped on well dispersed NDs through the thermal polymerization of the mixture composed of hexamethylenetetramine and ammonium chloride adsorbed on dispersed nanodiamonds, in which hexamethylenetetramine serves as both carbon nitride precursor and dispersing agent and the ammonium chloride acts as gas template. In comparison with the previously reported H-ND with carbon nitride layers close wrapped on ND formed by the thermal polymerization of a mixture composed of HTM and ND, the as-prepared ND-CN in this work demonstrates more exposed surface ketonic carbonyl groups and structural defects that serve as active sites for the direct dehydrogenation of ethylbenzene, owing to the more loose and porous carbon nitrides led by the gas template role of the added ammonium chloride. As a consequence, ND-CN may show much superior catalytic performance in the oxygen-/steam-free direct dehydrogenation.

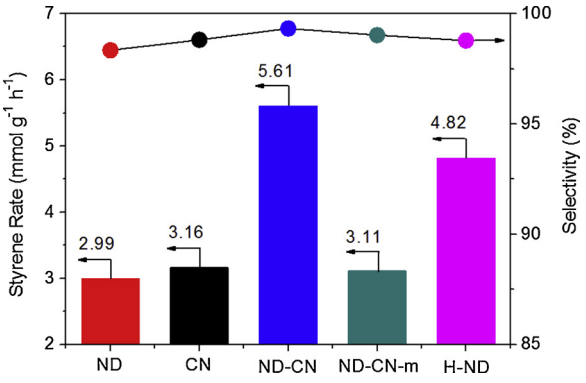


**Fig. 7.** Steady state styrene rate for direct dehydrogenation of ethylbenzene to styrene over the ND, CN, ND-CN, ND-CN-m and H-ND catalyst (20 h of time on stream). Reaction conditions: Catalyst (25 mg), 550 °C, 2.8% ethylbenzene in Ar, 10 ml $min^{-1}$ GHSV.

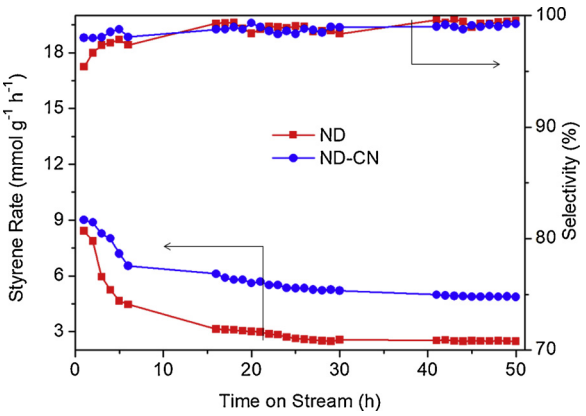


**Fig. 8.** The catalytic stability of the developed ND-CN catalyst for direct dehydrogenation of ethylbenzene to styrene under steam and oxidant-free conditions. Reaction conditions: Catalyst (25 mg), 550 °C, 2.8% ethylbenzene in Ar, 10 ml $min^{-1}$ GHSV.

### 3.2. Catalytic properties of the samples

The catalytic performance expressed in terms of styrene products per gram of catalyst per hours ($mmol_{ST}\,g^{-1}\,h^{-1}$) on the steady-state and the selectivity to styrene after 20 h reaction over ND, carbon nitride, ND-CN and H-ND were evaluated for the DDH reaction (Fig. 7). The weight of the catalyst in the reaction is 25 mg in all catalytic tests. ND-CN presents 5.61 mmol $g^{-1}\,h^{-1}$ of styrene rate (1.9 times higher than ND) with 99.3% selectivity, superior to the mixture of ND and CN (3.11 $mmol_{ST}\,g^{-1}\,h^{-1}$). The steady-state styrene rate of H-ND is 4.83 mmol $g^{-1}\,h^{-1}$ and the styrene selectivity is 98.8%, which is higher than ND (2.99 $mmol_{ST}\,g^{-1}\,h^{-1}$) but lower than ND-CN. For comparison, although NG-CN has a lower N content than H-ND, the developed ND-CN shows 1.2 times much higher styrene rate for oxygen and steam-free direct dehydrogenation of ethylbenzene than the previously reported carbon nitride encapsulated ND (H-ND) formed by the thermal polymerization of mixture composed of HTM and ND, respectively, ascribed the increased active sites containing defects and ketonic carbonyl groups and the not weakened synergistic effect of carbon nitride with ND that originating from the enlarging surface area and pore volume owing to the characteristic concerning loose porous structure of carbon nitride layers. Fig. 8 shows the long term stability of ND and ND-CN for DDH of ethylbenzene to styrene at 550 °C. From Fig. 7b, the results indicate that the conversion at the initial period, and then maintains a relatively stable value. It can be found that the selectivity gradually increases along with the time on stream, resulting from the suppressed formation of side-products including benzene and toluene

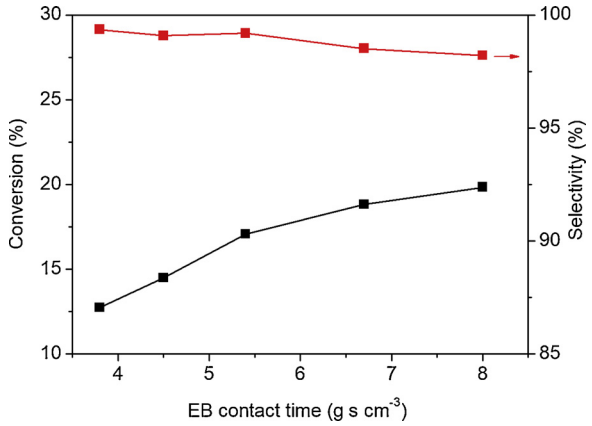


**Fig. 9.** Variation of conversion and selectivity with contact time over the developed ND-CN catalyst for direct dehydrogenation of ethylbenzene to styrene. Reaction conditions: Catalyst (25 mg), 550 °C, 2.8% ethylbenzene in Ar, variety of GHSV values (6, 8, 10, 12, and 14 ml $min^{-1}$).

through catalytic cracking of ethylbenzene by the surface phenolic hydroxyl group possibly owing to the decreased phenolic hydroxyl group along with the time on stream at 550 °C of high temperature. Fig. 9 presents the variation of conversion and selectivity with contact time. From Fig. 9, the extending contact time leads to a gradual increase in conversion. However, with the increase in contact time, only slight decreased selectivity can be observed if the contact time is not longer than 60.6 s. The further prolonged contact time lead to a dramatic decrease in selectivity. Therefore, the 60.6 s of appropriate contact time is required to obtain relatively high conversion with high selectivity.

## 4. Conclusions

In a summary, we have developed a simple, inexpensive and environmentally-friendly approach for synthesizing nanodiamond@carbon nitride hybrid with loose porous carbon nitride layers close wrapped on well dispersed NDs (ND-CN) through the thermal polymerization of the mixture composed of hexamethylenetetramine (HTM) and ammonium chloride adsorbed on dispersed nanodiamonds (ND), in which hexamethylenetetramine serves as both carbon nitride precursor and dispersing agent and the ammonium chloride acts as gas template. ND-CN shows 1.9 and 1.2 times much higher styrene rate for oxygen and steam-free direct dehydrogenation of ethylbenzene than ND and the previously reported carbon nitride layers encapsulated ND (H-ND) formed by the thermal polymerization of mixture composed of HTM and ND, respectively, ascribed the increased active sites containing defects and ketonic carbonyl groups and the not weakened synergistic effect of carbon nitride with ND that originating from the enlarging surface area and pore volume owing to the characteristic concerning loose porous structure of carbon nitride layers. This work presents a new way for designing and fabricating loose and porous carbon nitride-layer close-wrapped nanocarbon hybrid catalysts with excellent catalytic performance in diverse reactions.

## Acknowledgments

This work was financially supported by the National Natural Science Foundation of China (21676046 and U1610104) and the Chinese Ministry of Education via the Program for New Century Excellent Talents in Universities (NCET-12-0079).

## References

[1] W. Lei, Y.-P. Deng, G. Li, Z.P. Cano, X. Wang, D. Luo, Y. Liu, D. Wang, Z. Chen, ACS Catal. 8 (2018) 2464–2472.
[2] B.Y. Guan, S.L. Zhang, X.W. Lou, Angew. Chem. Int. Ed. 57 (2018) 6176–6180.

[3] N.P. Wickramaratne, J. Xu, M. Wang, L. Zhu, L. Dai, M. Jaroniec, Chem. Mater. 26 (2014) 2820–2828.
[4] C. Liu, X. Huang, J. Wang, H. Song, Y. Yang, Y. Liu, J. Li, L. Wang, C. Yu, Adv. Funct. Mater. 28 (2018) 1705253.
[5] R. Yuge, F. Nihey, K. Toyama, M. Yudasaka, Adv. Mater. 28 (2016) 7174–7177.
[6] V.N. Mochalin, O. Shenderova, D. Ho, Y. Gogotsi, Nat. Nanotechnol. 7 (2012) 11–23.
[7] D.A. Simpson, E. Morrisroe, J.M. McCoey, A.H. Lombard, D.C. Mendis, F. Treussart, L.T. Hall, S. Petrou, L.C. Hollenberg, ACS Nano 11 (2017) 12077–12086.
[8] Y. Liu, Y. Zhang, K. Cheng, X. Quan, X. Fan, Y. Su, S. Chen, H. Zhao, Y. Zhang, H. Yu, Angew. Chem. Int. Ed. 56 (2017) 15607–15611.
[9] T. Liu, S. Ali, B. Li, D.S. Su, ACS Catal. 7 (2017) 3779–3785.
[10] J. Zhang, D.S. Su, R. Blume, R. Schlögl, R. Wang, X. Yang, A. Gajović, Angew. Chem. Int. Ed. 49 (2010) 8640–8644.
[11] H. Liu, J. Diao, Q. Wang, S. Gu, T. Chen, C. Miao, W. Yang, D. Su, Chem. Commun. 50 (2014) 7810–7812.
[12] Y. Liu, H. Ba, J. Luo, K.-H. Wu, J.-M. Nhut, D.S. Su, C. Pham-Huu, Catal. Today 301 (2018) 38–47.
[13] Z. Zhao, Y. Dai, G. Ge, X. Guo, G. Wang, Green Chem. 17 (2015) 3723–3727.
[14] T.T. Thanh, H. Ba, L. Truong-Phuoc, J.-M. Nhut, O. Ersen, D. Begin, I. Janowska, D.L. Nguyen, P. Granger, C. Pham-Huu, J. Mater. Chem. A 2 (2014) 11349–11357.
[15] Z. Zhao, Y. Dai, G. Ge, Q. Mao, Z. Rong, G. Wang, ChemCatChem 7 (2015) 1070–1077.
[16] Z. Zhao, W. Li, Y. Dai, G. Ge, X. Guo, G. Wang, ACS Sustainable Chem. Eng. 3 (2015) 3355–3364.
[17] Z. Zhao, Y. Dai, J. Mater. Chem. A 2 (2014) 13442–13451.
[18] Z. Zhao, G. Ge, W. Li, X. Guo, G. Wang, Chin. J. Catal. 37 (2016) 644–670.
[19] R. Wang, X. Sun, B. Zhang, X. Sun, D. Su, Chem. Eur. J. 20 (2014) 6324–6331.
[20] G. Ge, X. Guo, C. Song, Z. Zhao, ACS Appl. Mater. Interf. 10 (2018) 18746–18753.
[21] H. Yu, R. Shi, Y. Zhao, T. Bian, Y. Zhao, C. Zhou, G.I. Waterhouse, L.Z. Wu, C.H. Tung, T. Zhang, Adv. Mater. 29 (2017) 1605148.
[22] P.P. Sharma, J. Wu, R.M. Yadav, M. Liu, C.J. Wright, C.S. Tiwary, B.I. Yakobson, J. Lou, P.M. Ajayan, X.D. Zhou, Angew. Chem. Int Ed.54 (2015) 13701–13705.
[23] Q. Liang, Z. Li, Z.H. Huang, F. Kang, Q.H. Yang, Adv. Funct. Mater. 25 (2015) 6885–6892.
[24] D. Zhang, Y. Guo, Z. Zhao, Appl. Catal. B Environ. 226 (2018) 1–9.
[25] C. Liu, Y. Zhang, F. Dong, A. Reshak, L. Ye, N. Pinna, C. Zeng, T. Zhang, H. Huang, Appl. Catal. B Environ. 203 (2017) 65–474.
[26] Y.P. Zhu, Y. Liu, Y.P. Liu, T.Z. Ren, T. Chen, Z.Y. Yuan, ChemCatChem 7 (2015) 2903–2909.
[27] X. Gu, W. Qi, S. Wu, Z. Sun, X. Xu, D. Su, Catal. Sci. Technol. 4 (2014) 1730–1733.
[28] Z. Li, J. Liu, C. Xia, F. Li, ACS Catal. 3 (2013) 2440–2448.
[29] Y. Chen, Z. Xiao, Y. Liu, L.-Z. Fan, J. Mater. Chem. A 5 (2017) 24178–24184.
[30] Z. Zhao, Y. Dai, G. Ge, X. Guo, G. Wang, Phys. Chem. Chem. Phys. 17 (2015) 18895–18899.
[31] X. Gao, Z. Chen, Y. Yao, M. Zhou, Y. Liu, J. Wang, W.D. Wu, X.D. Chen, Z. Wu, D. Zhao, Adv. Funct. Mater. 26 (2016) 6649–6661.
[32] F. Su, C.K. Poh, J.S. Chen, G. Xu, D. Wang, Q. Li, J. Lin, X.W. Lou, Energy Environ. Sci. 4 (2011) 717–724.
[33] J. Diao, Z. Feng, R. Huang, H. Liu, S.B.A. Hamid, D. Su, ChemSusChem 9 (2016) 662–666.
[34] Z. Ma, H. Zhang, Z. Yang, G. Ji, B. Yu, X. Liu, Z. Liu, Green Chem. 18 (2016) 1976–1982.
[35] X. Sun, R. Wang, D. Su, Chin. J. Catal. 34 (2013) 508–523.
[36] Z. Zhao, Y. Dai, J. Lin, G. Wang, Chem. Mater. 26 (2014) 3151–3161.
[37] X. Duan, Z. Ao, H. Sun, S. Indrawirawan, Y. Wang, J. Kang, F. Liang, Z.H. Zhu, S. Wang, ACS Appl. Mater. Interf. 7 (2015) 4169–4178.